5-2016

Maximizing ORC performance with optimal match of working fluid with system design

Kirtipal Barse
University of North Dakota, kirtipal.barse@und.edu

Michael Mann
University of North Dakota, michael.mann@und.edu

Maximizing ORC performance with optimal match of working fluid with system design

Kirtipal A. Barse[†], Michael D. Mann

Department of Chemical Engineering, University of North Dakota, Grand Forks, ND 58202

[†]Corresponding Author: Upson II Room 366Q, 243 Centennial Drive Stop 8153, Grand Forks, ND 58202, USA, Tel:+1701.777.4805, Email:kirtipal.barse@engr.und.edu

1. Abstract

This article compares constrained system design to non-constrained system design for the basic Organic Rankine Cycle (ORC). The 12 working fluids studied include eight dry-type, three isentropic, and one wet-type fluids. The ORC model was developed using Aspen HYSYS® and validated with data obtained from the literature. The constrained design compared the performance of working fluids for a fixed heat exchanger and turbine configuration. A non-constrained design was studied by altering the design specifications for the heat exchangers and turbine to match the working fluid. An energy and exergy analysis was performed using first and second law efficiency. The exergy analysis was also used to study exergy destruction across the ORC components. Cost analysis was performed by comparing the levelized cost of electricity (LCOE) for each working fluid in both designs.

It was observed that non-constrained design favored working fluids with higher critical temperatures. Switching from constrained to non-constrained design lowered the LCOE for higher critical temperature working fluids such as R601, R601a, R123, R245ca, R245fa, R600, and R236ea. R245ca, R601, and R236ea show 11%, 10%, and 9% decrease in LCOE, respectively. No significant change in efficiency is observed for lower critical temperature working fluids such as R236fa and R134a. Also, no increase in net power was observed for lower critical temperature working fluids, suggesting that modifying design does not affect the performance of ORC. LCOE increased for R600a, R152a, and R227ea and remained unchanged for R236fa and R134a.

Keywords: Organic Rankine cycle, Organic fluids, Thermodynamic Analysis, Exergy Analysis, Economics, Optimization

Nomenclature

T	Temperature (K)
P	Pressure (bar)
h	Enthalpy (kJ/kg)
s	Entropy (kJ/kg)
I	Irreversibility (kW)
W	Work (kW)
$\dot{m}$	Mass flow rate (kg/h)
$\dot{Q}$	Heat rate (kW)
UA	Thermal conductance (kJ/C-h)

Subscripts

e	Evaporator
c	Condenser
t	Turbine
p	Working fluid pump
0	Ambient
H	Heat source
L	Heat sink
tot	Total
1	Evaporator exit
2	Turbine exit
3	Condenser exit
4	Working fluid pump exit

Greek Symbols

η_I	Thermal Efficiency
η_{II}	Exergy Efficiency

2. Introduction

The Organic Rankine Cycle (ORC) is a promising technology for converting low-grade energy, including waste heat and low temperature geothermal resources, to electricity (Hung, Shai, Wang, and Polytechnic, 1997), (Schuster, Karellas, Kakaras, and Spliethoff, 2009). ORC has the same working principle as the conventional Rankine cycle and uses a low boiling point, high molecular weight organic fluid as the working fluid. Common organic fluids, such as R245fa, R134a, and isopentane, are used as working fluids for ORC (Desai and Bandyopadhyay, 2009), (Yamamoto, Furuhata, Arai, and Mori, 2001). Organic fluid vaporizes at low temperatures, allowing the extraction of energy from low temperature resources. ORC has been used to generate power from various low-temperature heat sources, such as waste heat, solar, biomass, and geothermal (Bruno, López-Villada, Letelier, Romera, and Coronas, 2008), (Cayer, Galanis, Desilets, Nesreddine, and Roy, 2009), (Manolakos, Kosmadakis, Kyritsis, and Papadakis, 2009), (Drescher and Brüggemann, 2007), (DiPippo, 2004). Commercial ORC systems are fabricated as modular systems and produce power from 50kW to 2MW. Figure 1 shows the schematic of a basic ORC. Usually the constrained design ORC comes with standard components; for example, the heat exchanger areas for evaporator and condenser are fixed. This may not allow the system to capture all the energy available at the resource. In addition, an ORC system designed for one working fluid may not be optimal for other working fluids. With this in mind, this article studies the effect of modifying system design on ORC performance. An attempt is made to maximize the performance of ORC with optimal matches of working fluids and system designs. The optimal match of working fluid with system design is achieved by modifying the ORC design. The ORC performance was studied using first and second law efficiency, net power, $/kW, and levelized cost of electricity (LCOE). Twelve working fluids were selected from the literature to compare the effect of constrained design to non-constrained design on an ORC plant in the base case.

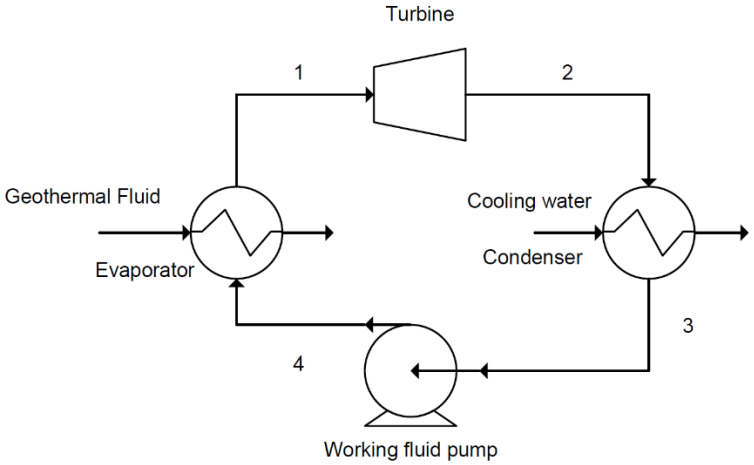

Figure 1. Schematic of basic Organic Rankine Cycle

Several authors have used thermal efficiency for ORC analysis (Hung, Wang, Kuo, Pei, and Tsai, 2010), (Quoilin, Lemort, and Lebrun, 2010), (Schuster, Karellas, and Aumann, 2010). The thermal analysis is based on the first law of thermodynamics, which takes into account the actual heat transferred to the system and determines the efficiency of the system. Other studies have used an exergy analysis, which is based on second law efficiency, to study the performance of

ORC (Heberle and Brüggemann, 2010), (Dai, Wang, and Gao, 2009), (Kanoglu and Bolatturk, 2008) , (Kanoglu, 2002), (DiPippo, 2004), (Yari, 2010), (B. F. Tchanche, Papadakis, Lambrinos, and Frangoudakis, 2009), (B. F. F. Tchanche, Lambrinos, Frangoudakis, and Papadakis, 2010), (Mago, Chamra, and Somayaji, 2007). The second law efficiency is the ratio of thermal efficiency to the maximum possible efficiency (Shengjun, Huaixin, and Tao, 2011). The second law efficiency serves as an approximation of the system's behavior under reversible operation. When the second law efficiency value approaches zero, the complete exergy of the resource is destroyed. As the efficiency approaches unity, the system behaves ideally and no exergy is destroyed.

Exergy is destroyed in the ORC plant by the fluid loss in the condenser, exergy of brine that is reinjected, the turbine pump losses, and the preheater vaporizer losses (Yari, 2010). Exergy destruction varies as the match degree varies between fluid streams in the evaporator (DiPippo, 2004). Shengjun used Exergy Destruction Factors (EDF) to compare the exergy destroyed across each component of the ORC (Shengjun et al., 2011). Larjola observed that higher power output is obtained when the working fluid matches the heat source (Larjola, 1995). This implies that decreasing the temperature difference between heat source and working fluid results in lower exergy destruction and thereby better performance. Tchanche *et al*. observed that for basic ORC the highest exergy destruction occurs in the evaporator, followed by the turbine, condenser, and pump (Tchanche *et al*., 2009). Aljundi observed that the highest and lowest exergy destruction occurs in the evaporator and pump, respectively (Aljundi, 2011).

The working fluid is the most important factor in determining the performance of the ORC. The slope of the working fluid saturation curves and environmental impact are the two major criteria to consider while selecting working fluid. The working fluids can be classified as wet, dry, and isentropic depending on their slope of saturation curves as shown in Figure 2. The wet fluid, after expansion in the turbine, contains saturated liquid and can condense. Dry and isentropic working fluids do not encounter this problem as the turbine exit stream is saturated or superheated vapor. Dry fluids have a positive slope and are the most preferred working fluid for ORC systems using low-grade heat sources (Desai and Bandyopadhyay, 2009). Mago *et al*. also concluded that dry organic fluids with higher boiling points have better efficiencies (Mago, Chamra, Srinivasan, and Somayaji, 2008). Liu *et al*. reported that the thermal efficiency of subcritical ORCs is a weak function of the critical temepraure of the working fluid (Liu, Chien, and Wang, 2004). Lee *et al*. concluded that the ORC system's efficiency is correlated to the working fluid's normal boiling point, critical pressure, and molecular weight (Lee, M J; Tien, D L; Shao, 1993).

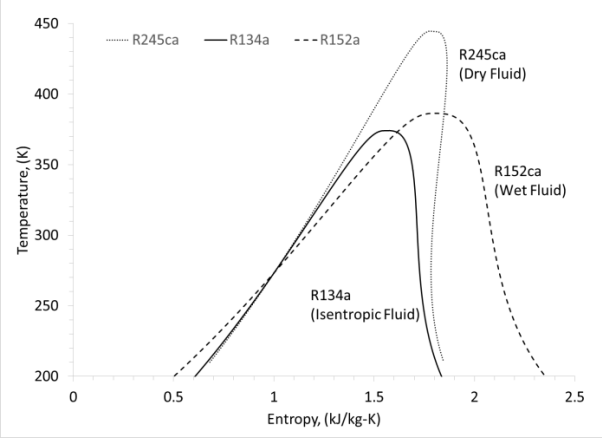

Figure 2. Types of working fluids

The investment cost of geothermal plants can be subdivided into surface equipment and the subsurface investment. Economics of the ORC system must be taken into account during optimization. An ORC system designed to deliver maximum efficiency may not be the most economical design. There is no precise information available for the capital cost of an ORC power plant. Also, the capital cost differs for various manufacturers and equipment sizes. The capital cost of low-temperature ORC systems is strongly dependent on the cost of the components such as heat exchangers, turbine, and pumps. The cost of these ORC components is directly related to their sizes (Lakew and Bolland, 2010). The maximum working pressure, the total heat transfer area, and the expander size strongly influence the economics of the ORC system(He et al., 2012) (He *et al*., 2012). The maximum working pressure is set by the corresponding saturation temperature of the working fluid in the evaporator. The saturation temperature is restricted by the resource temperature and the pinch point temperature in the evaporator. Many economic indicators have been suggested by several authors. The Levelized Cost of Electricity (LCOE) is defined as the cost of electricity generation over the life of the power plant. Several studies have used LCOE as an indicator for cost analysis (Shengjun *et al*., 2011), (El-Emam and Dincer, 2013).

3. Methodology

3.1. Model Development

The first step in this study was the development of a computer model of the ORC using Aspen HYSYS® with REFPROP as the property package. The ORC model was compared to plant data for validation.

The optimization of the ORC was performed to maximize the thermal efficiency. By the definition in equation 3, exergy efficiency is dependent on and directly proportional to the thermal efficiency. The optimization of the ORC was conducted using the "optimizer" tool in Aspen HYSYS®. The optimizer tool used thermal efficiency as the objective function and was set to maximize. The maximum working fluid pressure and mass flow rate were the two parameters varied to maximize the thermal efficiency. For constrained cases, the turbine power was set to 250kW and the pressure and the mass flow were varied to maximize thermal efficiency. The maximum values of thermal conductance for the heat exchangers were restricted to the value obtained from the model validation with the Chena Geothermal Power Plant. The maximum pressure possible for the working fluid is set by the saturation temperature and restricted by the source temperature.

For non-constrained cases, the thermal efficiency was maximized by varying the maximum pressure and mass flow rate of the working fluid. The turbine power was not restricted and was calculated under the optimized conditions. The thermal conductance for the heat exchangers was calculated under the optimized conditions. Table 1 shows the design differences between the constrained and non-constrained cases.

Table 1. Design for the constrained and non-constrained cases

	Constrained	Non-Constrained
Geothermal Resource Temperature (K)	372	372
Geothermal Resource Flow Rate, m^3/h	198.6	198.6
Cooling Water Temperature (K)	294	294

Maximum Gross Turbine Output, kW	250	Variable
Maximum Evaporator UA Value (kJ/C-h)	4.20×10^5	Variable
Maximum Condenser UA Value (kJ/C-h)	1.15×10^6	Variable
Maximum Turbine Size, m	0.15	Variable
Ambient Temperature, T_0 (K)	298	298
ΔT at Pinch Points in Heat Exchangers , (K)	6	6
ΔT of the Cooling Water, (K)	6	6
Turbine Efficiency	0.8	0.8
Maximum Pressure in the Cycle, bar	Variable	Variable
Maximum Flow Rate of Working Fluid, kg/h	Variable	Variable

3.2. Thermodynamic Analysis

The thermodynamic analysis is critical to studying the performance of the ORC under various operating conditions and working fluids. The first law efficiency, or thermal efficiency, is the ratio of net power produced to heat input to the system.

Thermal efficiency is expressed as:

$$\eta_I = \frac{(W_t - W_p)}{Q_e} \quad (1)$$

The maximum value of the first law efficiency is given by the Carnot efficiency.

$$\text{Carnot efficiency} = \left[1 - \frac{T_L}{T_H}\right] \quad (2)$$

where T_L and T_H are the temperatures of the heat sink and heat source, respectively.

The second law efficiency, as defined by (B. F. Tchanche *et al*., 2009) and (Aljundi, 2011), is expressed as:

$$\eta_{II} = \frac{\eta_I}{\left(1 - \frac{T_0}{T_H}\right)} \quad (3)$$

Exergy is the maximum work potential theoretically obtained from a source with respect to the surroundings (DiPippo, 2004). It can also be defined as the maximum possible work when a system undergoes a reversible process from the specified initial state to dead state. A dead state of a fluid occurs when the fluid is in equilibrium with the surroundings and there is no potential for doing work. The specific exergy of a stream defined by (DiPippo, 2004) is given as:

$$Specific\ Exergy_{stream} = (h - h_0) - T_0(s - s_0) \quad (4)$$

The equations used for thermodynamic analysis for each component are listed below (Shengjun *et al*., 2011). The following assumptions were made for the modeling of the ORC system.

- Each component is considered as a steady-state flow system.
- The specific heat of the source and sink are constant.
- The turbine and pump efficiencies are constant for all working fluids.

Evaporator

$$I_e = T_0 \dot{m}_{ORC} \left[(s_4 - s_1) - \left(\frac{h_4 - h_1}{T_H} \right) \right] \quad (5)$$

$$\dot{Q}_e = \dot{m}_{ORC} (h_4 - h_1) \quad (6)$$

Turbine

$$I_t = T_0 \dot{m}_{ORC} (s_2 - s_1) \quad (7)$$

$$W_t = \dot{m}_{ORC} (h_2 - h_1) \quad (8)$$

Refrigerant pump

$$I_p = T_0 \dot{m}_{ORC} (s_4 - s_3) \quad (9)$$

$$W_p = \dot{m}_{ORC} (h_4 - h_3) \quad (10)$$

Condenser

$$I_c = T_0 \dot{m}_{ORC} \left[(s_3 - s_2) - \left(\frac{h_3 - h_2}{T_L} \right) \right] \quad (11)$$

$$\dot{Q}_h = \dot{m}_{ORC} (h_3 - h_2) \quad (12)$$

Total irreversibility in the system

$$I_{tot} = I_p + I_e + I_t + I_c = T_0 \dot{m} \left[- \left(\frac{h_4 - h_1}{T_H} \right) - \left(\frac{h_3 - h_2}{T_L} \right) \right] \quad (13)$$

Net work obtained from the system

$$W_{net} = W_t - W_p \quad (14)$$

3.3. Working fluids

As listed in Table 2, eight dry fluids, three isentropic fluids, and one wet fluid were chosen for this study. The working fluids are arranged by decreasing critical temperature with R601 and R143a having highest and lowest critical temperature respectively. Only the subcritical region of the working fluids is considered for the study, and therefore all the fluids selected here have critical temperatures above the geothermal resource temperature.

Table 2. Thermodynamic Data for the Working Fluids

Working fluid	T_c (K)	P_c (bar)	NBP (K)	Type	GWP (100 yr)	ODP	ALT (yr)
R601	469.70	33.70	309.21	Dry	0	0	0
R601a	460.35	33.78	300.98	Dry	0	0	0
R123	456.83	36.61	300.97	Isentropic	77	0	1.3
R245ca	447.57	39.25	298.28	Dry	693	0	62
R245fa	427.16	36.51	288.29	Isentropic	1030	0	7.6
R600	425.13	37.96	272.66	Dry	20	0	0.02
R236ea	412.44	35.02	279.34	Dry	710	0	8
R600a	407.81	36.29	261.40	Dry	20	0	0.02
R236fa	398.07	32.00	271.71	Dry	9810	0	240
R152a	386.41	45.16	249.13	Wet	124	0	1.4
R227ea	374.90	29.25	256.81	Dry	3220	0	42
R134a	374.21	40.59	247.08	Isentropic	1430	0	14

3.4. Cost Analysis

The cost of the ORC components is directly related to their sizes (Lakew and Bolland, 2010). The total heat exchanger area consists of the evaporator and condenser area. The heat exchanger areas for each individual heat exchanger are obtained from the simulation results. The turbine size parameter is an indicator of turbine size (He *et al*., 2012), (Lakew and Bolland, 2010), (Khennich and Galanis, 2012).

The size parameter to calculate the expander size is given below.

$$SP = \frac{\sqrt{V}}{\sqrt[4]{\Delta H}} \quad (15)$$

where V (m^3/s) is the volumetric flow rate of the working fluid and ΔH (J/kg) is the specific enthalpy drop across the turbine.

The cost analysis was performed using capital cost expressed as installed equipment cost and LCOE. The installed equipment cost was obtained using Aspen HYSYS® for each individual working fluid for both the configurations. The equipment cost was divided by the net power produced for each case to express the equipment cost as $/kWh. The cost analysis performed in this study does not include any drilling or exploration costs for the geothermal resource. The LCOE was calculated using National Renewable Energy Laboratory's simple calculator (NREL, 2013). The values of the parameters used for the LCOE calculation are summarized in Table 3.

Table 3. Parameters for Levelized Cost of Electricity Calculation

Parameter	Value
Periods (year)	20
Discount Rate (%)	3
Capital Cost ($/kW)	Equipment cost/Net Power
Capacity Factor (%)	90
Constrained O&M Cost ($/kW-yr)	180
Variable O&M Cost ($/kWh)	0
Heat Rate (Btu/kWh)	0
Fuel Cost ($/kW)	0
Electricity Price (cents/kWh)	7
Cost Escalation Rate (%)	1.6%

The useful project life was assumed to be 20 years. The discount rate was adapted from the Federal Energy Management Program (Rushing, Kneifel, and Lippiatt, 2013). Geothermal plants are base-load power plants and generally have higher capacity factors. The capacity factor value was set at 90% based on the report published by NREL (Tidball, Bluestein, Rodriguez, and Knoke, 2010). The constrained and variable operation and maintenance costs, heat rate, and fuel cost were also selected based on the NREL report (Tidball *et al*., 2010). For renewable energy systems, the heat rate and fuel cost assumed by the model is 0. The electricity price and its commercial cost escalation rate was set at 7 cents per kWh and 1.6% for the Midwest region, respectively (NREL, 2013). The net power output, total heat exchanger area, size parameter, and LCOE were used as economic indicators.

4. Results and discussion

4.1. Model Validation against the Chena Geothermal Power Plant

The Chena geothermal power plant was built at the Chena Hot Springs, Alaska, in 2006. The plant uses United Technology's PureCycle® ORC unit, which produces 250kW gross power. The ORC model developed for this study was compared to the data obtained from Chena Geothermal Power Plant for validation. The ORC model was developed using the Aspen HYSYS® process simulator. The design conditions for the modeling were adapted from the published literature and are given in Table 4 (Holdmann, 2007), (Aneke, Agnew, and Underwood, 2011). Table 5 compares the results obtained from the simulation to the actual plant data for validation. It can be observed that the simulation results are comparable to the plant data.

Table 4. Design Conditions for the ORC Model

Geothermal fluid temperature (K)	346.5
Geothermal fluid mass flow rate (m^3/h)	120.4
Cooling water source temperature (K)	277.6
Cooing water source flow rate (m^3/h)	366.5
Working Fluid	R134a
Turbine efficiency	0.8
Turbine inlet pressure (bar)	16
Gross generator power (kW)	250

Table 5. Comparison of the Simulation Results

	Plant data	Simulation result	Relative error $\lvert\Delta X\rvert \times 100/X$
Turbine outlet pressure (bar)	4.39	4.4	0.64
Pump power (kW)	40	39.6	1.13
Geothermal exit temperature(K)	327.6	328.8	1.62
Cooling water exit temperature (K)	283.2	282.9	0.92
Working fluid mass flow rate (kg/s)	12.17	11.5	5.34
Net plant power (kW)	210	210.4	0.21
Thermal efficiency	0.08	0.085	6.29
Evaporator heat transfer rate (kWth)	2580	2475	4.07
Condenser heat transfer rate (kWth)	2360	2264	4.07
Evaporator UA value (kJ/C-hr)		4.20×10^5	
Condenser UA value (kJ/C-hr)		1.15×10^6	

Heat curves in Figure 3 and Figure 4 show the temperature profile and match degree between the thermal fluids in the heat exchangers. The match degree can be referred to as how parallel the heat curves are to each other. The match degree can be best shown using Figure 5, which compares the profile obtained in the evaporator to the ideal case profile. The dashed line shows the profile which could have been obtained if there were no phase change of the working fluid. If the pinch point did not exist, then the working fluid temperature would have been much higher. The difference between the solid and dashed line translates into lost potential in the evaporator. Therefore, it is essential to have a good profile match in the heat exchanger to minimize this lost potential.

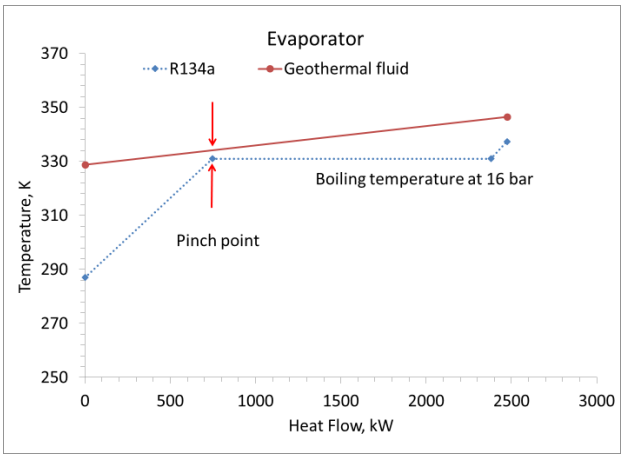

Figure 3. Heat flow diagram for the evaporator

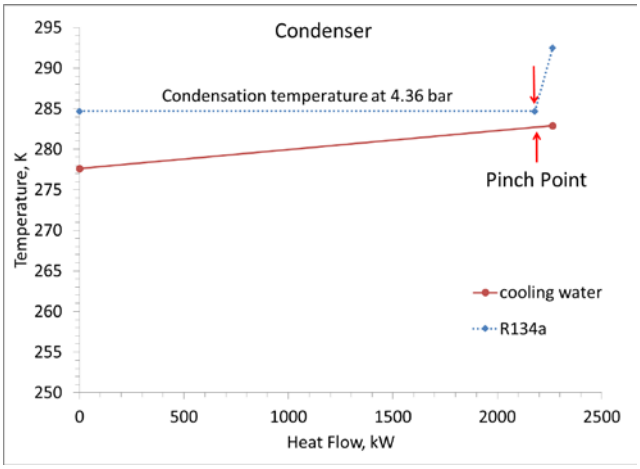

Figure 4. Heat flow diagram for the condenser

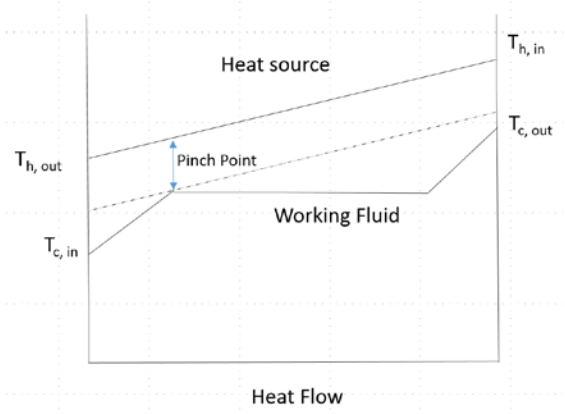

Figure 5. Heat flow diagram with working fluid exhibiting ideal match degree

4.2. Energy Analysis

Figure 6 shows the thermal efficiency of the working fluids in the constrained and non-constrained cases. Working fluids with higher critical temperatures display higher efficiency. The efficiency of R601 is 9.1%, 18% higher than the R134a efficiency. R601, R601a, R123, and R245ca have the highest thermal efficiencies. It can also be observed that for all working

fluids, the efficiency increased from switching from constrained to non-constrained designs. The efficiency of R601 jumped from 9.1% to 11.2%, an increase of 23%. The highest increase in efficiency, 25.5%, was observed for R600. Working fluids with lower critical temperatures did not show significant increases in efficiency. Thus, removing design constraints makes more sense for working fluids with higher critical temperatures.

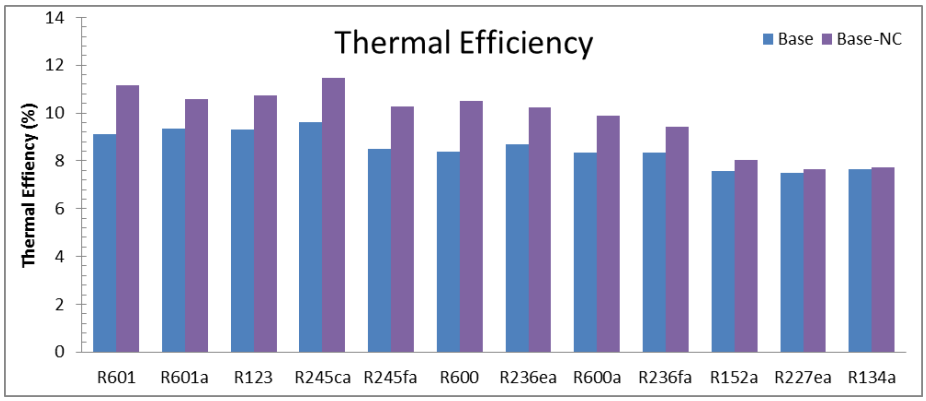

Figure 6. Thermal efficiency of the working fluids (listed by T_c from left to right)

Table 6 show the results for the two design for each working fluid. Modifying the design changed either the pressure in the system or the working fluid flow rate, and both in some cases. Working fluid pump power consumption is governed by pressure and working fluid flow rate in system. Working fluid with higher critical temperature such as R601, R601a and R123 required lower turbine pressure which explained the low power consumption of the working fluid pump. A higher working fluid flow rate in the case of R236ea and R236fa increased the pump power consumption. For R227ea, a combination of a higher working fluid flow rate and a high turbine pressure was responsible for the highest power consumption among all working fluid.

Table 6. Results for the constrained and non-constrained design case

	BASE				BASE-NC			
Working fluid	P_{in} (psia)	P_{out} (psia)	$\dot{m}_{ORC}$ (lb/hr)	W_p (kW)	P_{in} (psia)	P_{out} (psia)	$\dot{m}_{ORC}$ (lb/hr)	W_p (kW)
R601	64	16	4.7E+04	11	72	12	4.7E+04	14
R601a	90	20	4.6E+04	16	90	16	5.5E+04	20
R123	95	20	9.2E+04	15	97	15	9.4E+04	16
R245ca	110	22	8.0E+04	16	115	16	9.5E+04	21
R245fa	116	28	9.0E+04	18	153	26	9.0E+04	26
R600	163	47	4.6E+04	29	193	39	4.0E+04	33
R236ea	139	33	1.0E+05	23	190	32	1.1E+05	38
R600a	182	56	4.9E+04	34	240	53	4.4E+04	46
R236fa	156	40	1.1E+05	28	221	42	1.0E+05	41
R152a	250	86	6.2E+04	36	355	97	6.4E+04	56
R227ea	240	66	1.3E+05	52	283	70	1.3E+05	64
R134a	302	98	9.4E+04	49	311	99	9.5E+04	52

Figure 7 plots the critical temperature of the working fluids against the corresponding first law efficiency obtained by simulation. It can be observed that the efficiency increased as the critical temperature of the working fluids increased. Aljundi found similar results, demonstrating strong correlation between critical temperature and efficiency (Aljundi, 2011). A similar correlation was also observed for the plot of first law efficiency and normal boiling point of fluids in Figure 8.

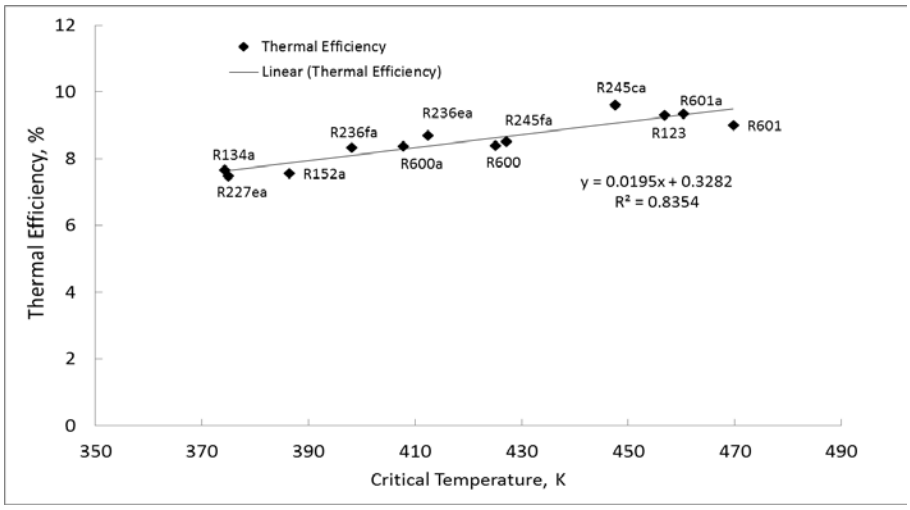

Figure 7. Thermal efficiency as a function of critical temperature of working fluids

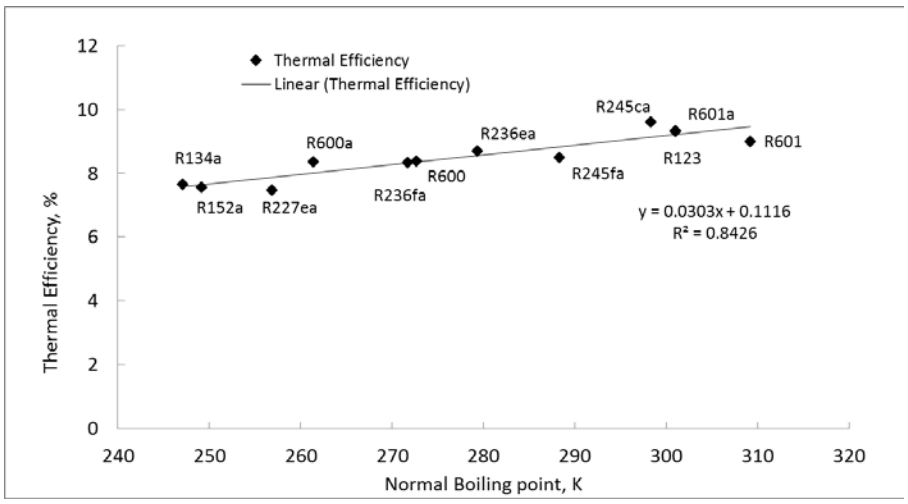

Figure 8. Thermal efficiency as a function of normal boiling point of working fluids

4.3. Exergy Analysis

Exergy analysis is based on the second law of thermodynamics and measures the irreversibilities in the cycle. Exergy analysis reveals the degradation of the system's ability to perform work with respect to the surroundings (Yari, 2010). Figure 9 compares the exergy efficiency for the working fluids for the constrained and non-constrained designs. Exergy efficiency is a measure of performance relative to performance under reversible conditions. Similar to the thermal efficiency, exergy efficiency is highest for R245ca and lowest for R152a.

It can be observed that second law efficiency follows the same trend as the first law efficiency since the second law efficiency is the ratio of the first law efficiency to the maximum work possible. For a given heat source and ambient conditions, the maximum work remains constant. Therefore, second law efficiency is directly proportional to first law efficiency. Exergy efficiency of R245ca was 48.4% and is 37% higher than that of R152a. DiPippo reported geothermal plants having exergy efficiencies of 40% or greater (DiPippo, 2004).

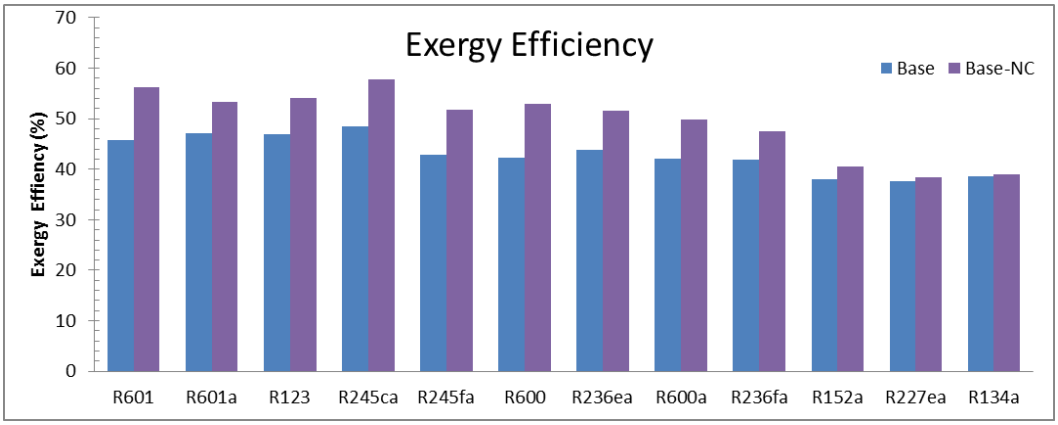

Figure 9. Exergy efficiency of the working fluids (listed by T_c from left to right)

Exergy analysis can be used to identify process deficiencies and allows a choice of system components that represent the most potential for improving the overall efficiency of the entire system. Figure 10 shows the exergy destruction rate across the each component for the ORC. The rate of exergy destruction is highest in the evaporator, followed by the condenser, turbine, and pump. The results reported here are in agreement with previous studies conducted by various authors. Overall, exergy analysis suggests that highest work potential is lost in the evaporator and condenser. Similar observations has been made by other authors (El-Emam and Dincer, 2013), (Mago *et al.*, 2008). For R600, as shown in Figure 10, 77% of the exergy destruction occurs in the evaporator and condenser combined for the constrained case. For non-constrained cases, the combined exergy destruction in the evaporator and condenser decreased to 63%, suggesting removing design constraints reduces exergy destruction in ORC. The heat exchangers represent the components with the most potential for improving the overall cycle efficiency.

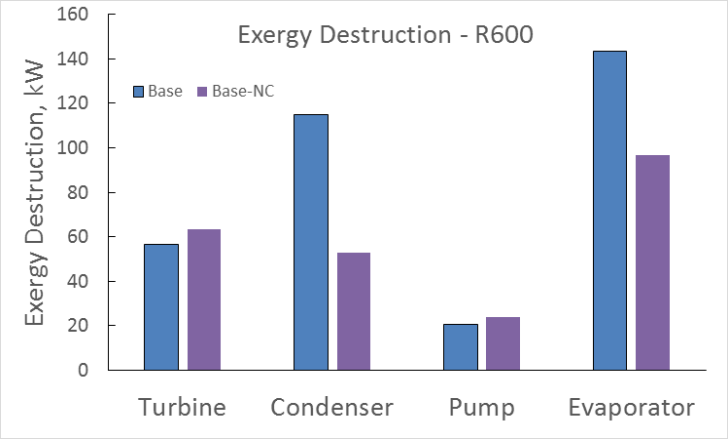

Figure 10. Exergy destruction across ORC components

4.4. Cost Analysis

The previous sections demonstrated that the ORC efficiency changes with working fluid and configuration. The change in efficiency occurs due to changes in thermodynamic conditions of the cycle and affects the power generated, equipment sizing, and hence, economics of the overall plant. A cycle maximizing the efficiency may not be the most cost effective mode of operation. Therefore, it is necessary to study the economics of the cycle, and a balance between efficiency and cost must be achieved. Figure 11 shows the net power for the working fluids in constrained and non-constrained designs. For the constrained design, the turbine gross power is constant at 250kW and the pump power is dependent on the working fluid and cycle pressure. Therefore, net power is not the same for all working fluids for constrained design. Working fluids with higher critical temperatures generate higher net power. For the non-constrained design, R245ca generates the highest net power value at 343kW. This translates into a 46% increase in the net power compared to constrained ORC design. The increase in net power is not significant for lower critical temperature working fluids, suggesting that a change in ORC design may not affect the performance for those fluids.

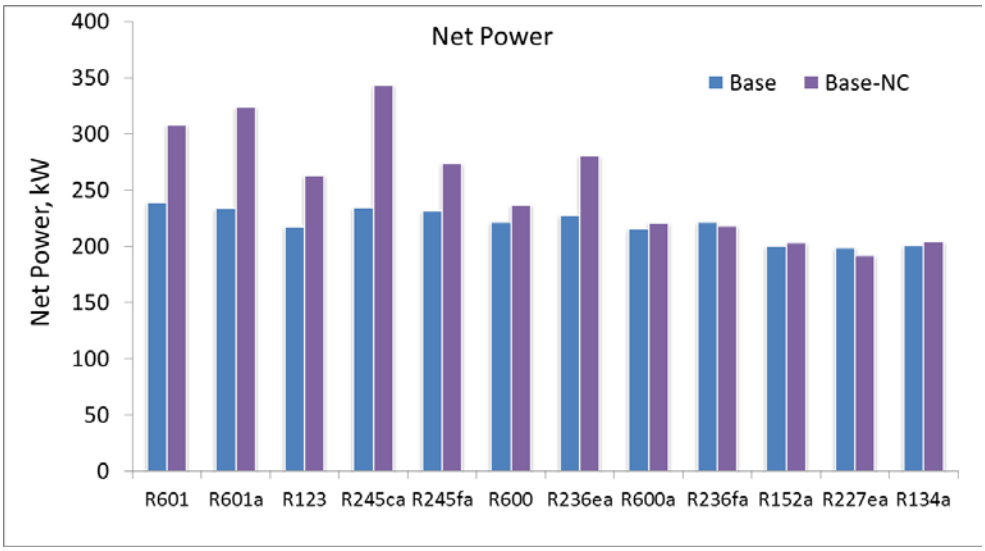

Figure 11. Net power for the working fluids

The size of the expander is represented by a size parameter and is shown in Figure 12. The turbine size parameter is an indicator of turbine size and allows for a comparison of the different designs. A higher value of size parameter indicates a bigger turbine size. A general increasing trend is observed for size parameter as the critical temperature decreases. However, more variability is observed in the results obtained. The increase in size parameter from R601a to R134a can be attributed to the increase in mass flow rates of working fluid and decreased turbine output. For comparison, the size parameter for the Chena power plant is 0.16. Size parameters exceed 0.16 for R236ea, R236fa, R227ea, and R134a.

Figure 12. Size parameters for the working fluids

Table 7 lists the calculated LCOE for all cases. LCOE was calculated using NREL's simple LCOE calculator. The lowest LCOE, 3.9 cents/kWh, was observed for R245ca under the non-constrained design. R601a and R236ea have the next lowest LCOE at 4.1 cents/kWh for the non-constrained design. R245ca, R601a, and R601 displayed the highest net power in non-constrained design. The LCOE was estimated to be 3.9, 4.1, and 4.2 cents/kWh, respectively. This shows that the LCOE is correlated with the net power generated by the cycle and is typically the highest for the base non-constrained design. R245ca, R601, and R236ea show 11%, 10%, and 9% decrease in LCOE, respectively. As compared to the constrained case, R600a, R227ea, and R152a show 4.3%, 4.1%, and 3.9% increases in LCOE, respectively. With non-constrained designs, R236fa and R134a show no change in LCOE as compared to the constrained design. Based on the overall cost analysis, R245ca, R601a, R601, R245fa and R236ea show better performance among the 12 selected fluids in non-constrained design. This also suggests that making design changes has the most economic potential for higher critical temperature working fluids.

Table 7 Levelized cost of electricity (cents/kWh)

Working Fluid	BASE	BASE-NC
R601	4.7	4.2

R601a	4.4	4.1
R123	4.6	4.3
R245ca	4.4	3.9
R245fa	4.5	4.2
R600	4.6	4.5
R236ea	4.5	4.1
R600a	4.7	4.9
R236fa	4.6	4.6
R152a	5.1	5.3
R227ea	4.9	5.1
R134a	4.9	4.9

5. Conclusions

An ORC model was successfully developed using Aspen HYSYS® process simulator and validated using the data from the Chena geothermal power plant. Results show that there is a strong correlation between the critical temperature of the working fluid and the efficiency of the working fluids. The choice of working fluids and system design affect the performance and economics of the ORC. Optimizing the system design can lead to an increase in thermal efficiency as high as 25% in the case of R600. On the other hand, R227ea and R134a did not show significant increases in thermal efficiency. The decrease in LCOE can be as low as 11% for R245ca by using a non-constrained design. For R600a, R152a, and R227ea, the LCOE was similar for the constrained design as compared to the optimized design. Working fluids with higher critical temperatures benefit most from non-constrained designs and subsequently show lower LCOE compared to constrained system designs. Working fluids with lower critical temperatures do not show significant improvement in performance and economics using the non-constrained design.

Acknowledgments

This work was supported by the Department of Energy Geothermal Technologies Office and Petroleum Research Education and Entrepreneurship Center of Excellence at the University of North Dakota.

References

Aljundi, I. H. (2011). Effect of dry hydrocarbons and critical point temperature on the efficiencies of organic Rankine cycle. *Renewable Energy*, *36*(4), 1196–1202. http://doi.org/10.1016/j.renene.2010.09.022

Aneke, M., Agnew, B., & Underwood, C. (2011). Performance analysis of the Chena binary geothermal power plant. *Applied Thermal Engineering*, *31*(10), 1825–1832. http://doi.org/10.1016/j.applthermaleng.2011.02.028

Bruno, J. C., López-Villada, J., Letelier, E., Romera, S., & Coronas, A. (2008). Modelling and optimisation of solar organic rankine cycle engines for reverse osmosis desalination. *Applied Thermal Engineering*, *28*(17-18), 2212–2226. http://doi.org/10.1016/j.applthermaleng.2007.12.022

Cayer, E., Galanis, N., Desilets, M., Nesreddine, H., & Roy, P. (2009). Analysis of a carbon dioxide transcritical power cycle using a low temperature source. *Applied Energy*, *86*(7-8), 1055–1063. http://doi.org/10.1016/j.apenergy.2008.09.018

Dai, Y., Wang, J., & Gao, L. (2009). Parametric optimization and comparative study of organic Rankine cycle (ORC) for low grade waste heat recovery. *Energy Conversion and Management*, *50*(3), 576–582. http://doi.org/10.1016/j.enconman.2008.10.018

Desai, N. B., & Bandyopadhyay, S. (2009). Process integration of organic Rankine cycle. *Energy*, *34*(10), 1674–1686. http://doi.org/10.1016/j.energy.2009.04.037

DiPippo, R. (2004). Second Law assessment of binary plants generating power from low-temperature geothermal fluids. *Geothermics*, *33*(5), 565–586. http://doi.org/10.1016/j.geothermics.2003.10.003

Drescher, U., & Brüggemann, D. (2007). Fluid selection for the Organic Rankine Cycle (ORC) in biomass power and heat plants. *Applied Thermal Engineering*, *27*(1), 223–228. http://doi.org/10.1016/j.applthermaleng.2006.04.024

El-Emam, R. S., & Dincer, I. (2013). Exergy and exergoeconomic analyses and optimization of geothermal organic Rankine cycle. *Applied Thermal Engineering*, *59*(1-2), 435–444. http://doi.org/10.1016/j.applthermaleng.2013.06.005

He, C., Liu, C., Gao, H., Xie, H., Li, Y., Wu, S., & Xu, J. (2012). The optimal evaporation temperature and working fluids for subcritical organic Rankine cycle. *Energy*, *38*(1), 136–143. http://doi.org/10.1016/j.energy.2011.12.022

Heberle, F., & Brüggemann, D. (2010). Exergy based fluid selection for a geothermal Organic Rankine Cycle for combined heat and power generation. *Applied Thermal Engineering*, *30*(11-12), 1326–1332. http://doi.org/10.1016/j.applthermaleng.2010.02.012

Holdmann, G. (2007). Renewable baseload energy: Geothermal Heat Pumps to engineered reservoirs. In *Geothermal Resource Council - Annual Meeting of the Geothermal Resource Council* (pp. 515–519).

Hung, T. C., Shai, T. ., Wang, S. K., & Polytechnic, K. (1997). A REVIEW OF ORGANIC RANKINE CYCLES (ORCs) FOR THE RECOVERY OF LOW-GRADE WASTE HEAT. *Energy*, *22*(7), 661–667.

Hung, T. C., Wang, S. K., Kuo, C. H., Pei, B. S., & Tsai, K. F. (2010). A study of organic working fluids on system efficiency of an ORC using low-grade energy sources. *Energy*, *35*(3), 1403–1411. http://doi.org/10.1016/j.energy.2009.11.025

Kanoglu, M. (2002). Exergy analysis of a dual-level binary geothermal power plant. *Geothermics*, *31*(6), 709–724. http://doi.org/10.1016/S0375-6505(02)00032-9

Kanoglu, M., & Bolatturk, A. (2008). Performance and parametric investigation of a binary geothermal power plant by exergy. *Renewable Energy*, *33*(11), 2366–2374. http://doi.org/10.1016/j.renene.2008.01.017

Khennich, M., & Galanis, N. (2012). Thermodynamic analysis and optimization of power cycles using a fi nite low temperature heat source. *Entropy*, *14*(March 2011), 871–885. http://doi.org/10.1002/er

Lakew, A. A., & Bolland, O. (2010). Working fluids for low-temperature heat source. *Applied Thermal Engineering*, *30*(10), 1262–1268. http://doi.org/10.1016/j.applthermaleng.2010.02.009

Larjola, J. (1995). Electricity from industrial waste heat using high-speed organic Rankine cycle (ORC). *Int. J. Production Economics*, *41*, 227–235.

Lee, M J; Tien, D L; Shao, C. T. (1993). Thermophysical capability of ozone safe working fluids for an organic rankine cycle system. *Heat Recovery Systems & CHP*, *13*(5), 409–418.

Liu, B.-T., Chien, K.-H., & Wang, C.-C. (2004). Effect of working fluids on organic Rankine cycle for waste heat recovery. *Energy*, *29*(8), 1207–1217. http://doi.org/10.1016/j.energy.2004.01.004

Mago, P. J., Chamra, L. M., & Somayaji, C. (2007). Performance analysis of different working fluids for use in organic Rankine cycles. *Proceedings of the Institution of Mechanical Engineers, Part A: Journal of Power and Energy*, *221*(3), 255–265. http://doi.org/10.1243/09576509JPE372

Mago, P. J., Chamra, L. M., Srinivasan, K., & Somayaji, C. (2008). An examination of regenerative organic Rankine cycles using dry fluids. *Applied Thermal Engineering*, *28*(8-9), 998–1007. http://doi.org/10.1016/j.applthermaleng.2007.06.025

Manolakos, D., Kosmadakis, G., Kyritsis, S., & Papadakis, G. (2009). Identification of behaviour and evaluation of performance of small scale, low-temperature Organic Rankine Cycle system coupled with a RO desalination unit. *Energy*, *34*(6), 767–774. http://doi.org/10.1016/j.energy.2009.02.008

NREL. (2013). No Title. Retrieved from http://www.nrel.gov/analysis/tech_lcoe.html

Quoilin, S., Lemort, V., & Lebrun, J. (2010). Experimental study and modeling of an Organic Rankine Cycle using scroll expander. *Applied Energy*, *87*(4), 1260–1268. http://doi.org/10.1016/j.apenergy.2009.06.026

Rushing, A. S., Kneifel, J. D., & Lippiatt, B. C. (2013). *Energy Price Indices and Discount Factors for Life-Cycle Cost Analysis – 2013 Annual Supplement to NIST Handbook 135 and NBS Special Publication 709*.

Schuster, a., Karellas, S., & Aumann, R. (2010). Efficiency optimization potential in supercritical Organic Rankine Cycles. *Energy*, *35*(2), 1033–1039. http://doi.org/10.1016/j.energy.2009.06.019

Schuster, a., Karellas, S., Kakaras, E., & Spliethoff, H. (2009). Energetic and economic investigation of Organic Rankine Cycle applications. *Applied Thermal Engineering*, *29*(8-9), 1809–1817. http://doi.org/10.1016/j.applthermaleng.2008.08.016

Shengjun, Z., Huaixin, W., & Tao, G. (2011). Performance comparison and parametric optimization of subcritical Organic Rankine Cycle (ORC) and transcritical power cycle system for low-temperature geothermal power generation. *Applied Energy*, *88*(8), 2740–2754. http://doi.org/10.1016/j.apenergy.2011.02.034

Tchanche, B. F. F., Lambrinos, G., Frangoudakis, a., & Papadakis, G. (2010). Exergy analysis of micro-organic Rankine power cycles for a small scale solar driven reverse osmosis desalination system. *Applied Energy*, *87*(4), 1295–1306. http://doi.org/10.1016/j.apenergy.2009.07.011

Tchanche, B. F., Papadakis, G., Lambrinos, G., & Frangoudakis, A. (2009). Fluid selection for a low-temperature solar organic Rankine cycle. *Applied Thermal Engineering*, *29*(11-12), 2468–2476. http://doi.org/10.1016/j.applthermaleng.2008.12.025

Tidball, R., Bluestein, J., Rodriguez, N., & Knoke, S. (2010). *Cost and Performance Assumptions for Modeling Electricity Generation Technologies Cost and Performance Assumptions for Modeling Electricity Generation Technologies*.

Yamamoto, T., Furuhata, T., Arai, N., & Mori, K. (2001). Design and testing of the Organic Rankine Cycle. *Energy*, *26*(3), 239–251. http://doi.org/10.1016/S0360-5442(00)00063-3

Yari, M. (2010). Exergetic analysis of various types of geothermal power plants. *Renewable Energy*, *35*(1), 112–121. http://doi.org/10.1016/j.renene.2009.07.023